

REFLECTIVITY AND PHASE CONTROL RESEARCH FOR SUPERRESOLUTION ENHANCEMENT VIA THE THIN FILMS MISMATCH

P. F. Cao, L. Cheng, Y. E. Li, X. P. Zhang, Q. Q. Meng
and W. J. Kong

School of Information Science and Engineering
Lanzhou University
Lanzhou 730000, China

Abstract—In this work, based on the principle of the electromagnetic reflection and transmission, we first present a theoretical analysis of a super-resolving lens with anti-reflection and phase control coatings (ARPC). This ARPC is capable of reducing the reflectivity of superlens surface and making phase difference approaching zero. The principle of ARPC is discussed in detail and the engineer condition for super-resolution imaging is obtained and the best range of the permittivity of ARPC coatings is obtained. The results demonstrate that the subwavelength resolution of our lens with ARPC has been enhanced. Such remarkable imaging capability using ARPC promises new potential for nanoscale imaging and lithography.

1. INTRODUCTION

In 2000, Pendry [1] showed that a simple noble metal slab, as named left-handed material [2–6], which was called superlens, displayed negative refraction [7–12] of the Poynting vector for TM polarized light and was capable of enhancing evanescent waves. So far, many approaches of imaging beyond the diffraction limit with superlens have been reported [13–18]. The performance limit of the metallic superlens was associated with the intrinsic losses of metal. Many theories and experiments demonstrate that the phase control of the superlens is profoundly important in realizing nano-scale imaging beyond the diffraction limit [19, 20]. The real part (ϵ') of permittivity of the metal slab has been preferably index matched to the host material (free space

in this case, $\varepsilon' = -\varepsilon_h = -1$) and the image part of metal's permittivity (ε'') is considered to prevent ideal reconstruction of the image [21], which is regarded as an ultimate limitation to a near field perfect lens. Recently, Ref. [22, 23] have presented some solution methods, which can enhance the resolving capabilities by tuning the wavelength of the incident light. However, the transmittance through a metal film is quite low and decreases exponentially with the thickness of the metal film. The low transmittance of metals limited their operating range to wavelengths in the vicinity of the plasma frequency and leads to the low intensity in the image plane, which cause the low image contrast and the low resolution. The transmittance can be improved with multilayer metal/dielectric stack [24, 25], but the original proposal was based on very thin layers (5 nm thick) which are difficult to fabricate.

In this manuscript, an Anti-Reflection and Phase Control coatings superlens (ARPC-superlens) model is firstly presented to get better values of transmittance and resolving capabilities. Based on electromagnetic theory, the matching conditions and constraint relations are discussed. Simultaneously, when the minimum reflectivity and the minimum phase difference are satisfied, the best range of the permittivity of ARPC coatings is obtained. Utilizing the numerical analysis, phase transfer function (PTF), light intensity distributions and image contrast of ARPC-superlens are compared with the superlens without ARPC. All these research results indicate that the super-resolution can be remarkable improved by utilizing ARPC.

2. ANTI-REFLECTION AND PHASE CONTROL COATINGS SUPERLENS

The proposed ARPC-superlens model is made of a superlens and two thin films, as shown in Figure 1. Suppose that in vacuum, our model

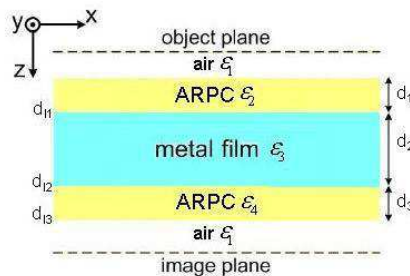


Figure 1. The ARPC-superlens sample structure.

is located in x - z plane between $z = 0$ and $z = d_{l3}$; the thickness of two ARPC films and Ag slab are d_1 , d_3 and d_2 , respectively. The normal wave vector is along z -axis. We define five regions according to the z values. Region I and V are for $z < 0$ and $z > d_{l3}$, i.e., the region of the air, which permittivity is $\varepsilon_1 = 1$; region II and IV cover $0 < z < d_{l1}$ and $d_{l2} < z < d_{l3}$, i.e., the region of the ARPC films, which permittivity are ε_2 and ε_4 , respectively; region III is $d_{l1} < z < d_{l2}$, i.e., the region of the superlens, which permittivity is ε_3 ($\varepsilon_3 = \varepsilon' + i\varepsilon''$).

We assume k_x is the transverse wave vector and k_z^j ($j = 1 \sim 5$) is the z -direction wave number in j -region, $k_x^2 + (k_z^j)^2 = \varepsilon_j \mu (\omega/c)^2$. Under the condition of high spatial frequency $\omega \ll c_0 \sqrt{k_x^2}$, $k_z^j = \sqrt{\varepsilon_j \mu (\omega/c)^2 - k_x^2} \simeq jk_x$. Assumed $d_1 + d_3 = d_2$ [22], when TM mode light is incident, the electrical field and the magnetic field in the five regions can be expressed as:

$$\begin{aligned}
 H_1 &= e^{ik_{1x}x} \left(e^{ik_z^{(1)}z} + R e^{-ik_z^{(1)}z} \right) \\
 E_{1x} &= \frac{-k_z^{(1)}}{\omega \varepsilon_1} e^{ik_{1x}x} \left(e^{ik_z^{(1)}z} - R e^{-ik_z^{(1)}z} \right) \\
 H_2 &= e^{ik_{2x}x} \left(A_1 e^{ik_z^{(2)}z} + A_2 e^{-ik_z^{(2)}z} \right) \\
 E_{2x} &= \frac{-k_z^{(2)}}{\omega \varepsilon_2} e^{ik_{2x}x} \left(A_1 e^{ik_z^{(2)}z} - A_2 e^{-ik_z^{(2)}z} \right) \\
 H_3 &= e^{ik_{3x}x} \left(B_1 e^{ik_z^{(3)}z} + B_2 e^{-ik_z^{(3)}z} \right) \\
 E_{3x} &= \frac{-k_z^{(3)}}{\omega \varepsilon_3} e^{ik_{3x}x} \left(B_1 e^{ik_z^{(3)}z} - B_2 e^{-ik_z^{(3)}z} \right) \\
 H_4 &= e^{ik_{4x}x} \left(C_1 e^{ik_z^{(4)}z} + C_2 e^{-ik_z^{(4)}z} \right) \\
 E_{4x} &= \frac{-k_z^{(4)}}{\omega \varepsilon_4} e^{ik_{4x}x} \left(C_1 e^{ik_z^{(4)}z} - C_2 e^{-ik_z^{(4)}z} \right) \\
 H_5 &= e^{ik_{1x}x} T e^{ik_z^{(1)}z} \\
 E_{5x} &= \frac{-k_z^{(1)}}{\omega \varepsilon_1} e^{ik_{1x}x} T e^{ik_z^{(1)}z}
 \end{aligned}$$

where R and T denote the reflection and transmission coefficients, respectively, $A_{1,2}$ and $C_{1,2}$ are coefficients for the waves inside the ARPC, respectively, and $B_{1,2}$ are coefficients for the waves inside the superlens.

In the present case, the boundary conditions state that k_{ix} , and

E_{ix} and H_i ($i = 1 \sim 5$) are continuous across the boundaries at $z = 0$, $z = d_{l1}$, $z = d_{l2}$, and $z = d_{l3}$, we can get the matrix form by using the electromagnetic theory method concerned as Ref. [26]:

$$\begin{pmatrix} 1 \\ R \end{pmatrix} = \frac{T}{16\varepsilon_2\varepsilon_3\varepsilon_4} \begin{pmatrix} (H_1+H_8)+(H_2+H_5)+(H_3+H_6)+(H_4+H_7) \\ (J_1+J_8)+(J_2+J_5)+(J_3+J_6)+(J_4+J_7) \end{pmatrix} \quad (1)$$

where

$$\begin{aligned} H_1 &= D'_1 E'_1 F'_1 G'_1 e^{\vartheta_1} = D_1 G_1 (\varepsilon_3^2 + (\varepsilon_4 + \varepsilon_2) \varepsilon_3 + \varepsilon_2 \varepsilon_4) e^{\vartheta_1} \\ H_2 &= D'_1 E'_1 F'_2 G'_2 e^{\vartheta_2} = D_1 G_2 (-\varepsilon_3^2 + (\varepsilon_4 - \varepsilon_2) \varepsilon_3 + \varepsilon_2 \varepsilon_4) e^{\vartheta_2} \\ H_3 &= D'_1 E'_2 F'_2 G'_1 e^{\vartheta_3} = D_1 G_1 (-\varepsilon_3^2 + (\varepsilon_4 + \varepsilon_2) \varepsilon_3 - \varepsilon_2 \varepsilon_4) e^{\vartheta_3} \\ H_4 &= D'_1 E'_2 F'_1 G'_2 e^{\vartheta_4} = D_1 G_2 (\varepsilon_3^2 + (\varepsilon_4 - \varepsilon_2) \varepsilon_3 - \varepsilon_2 \varepsilon_4) e^{\vartheta_4} \\ H_5 &= D'_2 E'_2 F'_1 G'_1 e^{\vartheta_5} = D_2 G_1 (\varepsilon_3^2 + (\varepsilon_4 - \varepsilon_2) \varepsilon_3 - \varepsilon_2 \varepsilon_4) e^{\vartheta_5} \\ H_6 &= D'_2 E'_2 F'_2 G'_2 e^{\vartheta_6} = D_2 G_2 (-\varepsilon_3^2 + (\varepsilon_4 + \varepsilon_2) \varepsilon_3 - \varepsilon_2 \varepsilon_4) e^{\vartheta_6} \\ H_7 &= D'_2 E'_1 F'_2 G'_1 e^{\vartheta_7} = D_2 G_1 (-\varepsilon_3^2 + (\varepsilon_4 - \varepsilon_2) \varepsilon_3 + \varepsilon_2 \varepsilon_4) e^{\vartheta_7} \\ H_8 &= D'_2 E'_1 F'_1 G'_2 e^{\vartheta_8} = D_2 G_2 (\varepsilon_3^2 + (\varepsilon_4 + \varepsilon_2) \varepsilon_3 + \varepsilon_2 \varepsilon_4) e^{\vartheta_8} \\ J_1 &= D'_2 E'_1 F'_1 G'_1 e^{\vartheta_1} = D_2 G_1 (\varepsilon_3^2 + (\varepsilon_4 + \varepsilon_2) \varepsilon_3 + \varepsilon_2 \varepsilon_4) e^{\vartheta_1} \\ J_2 &= D'_2 E'_1 F'_2 G'_2 e^{\vartheta_2} = D_2 G_2 (-\varepsilon_3^2 + (\varepsilon_4 - \varepsilon_2) \varepsilon_3 + \varepsilon_2 \varepsilon_4) e^{\vartheta_2} \\ J_3 &= D'_2 E'_2 F'_2 G'_1 e^{\vartheta_3} = D_2 G_1 (-\varepsilon_3^2 + (\varepsilon_4 + \varepsilon_2) \varepsilon_3 - \varepsilon_2 \varepsilon_4) e^{\vartheta_3} \\ J_4 &= D'_2 E'_2 F'_1 G'_2 e^{\vartheta_4} = D_2 G_2 (\varepsilon_3^2 + (\varepsilon_4 - \varepsilon_2) \varepsilon_3 - \varepsilon_2 \varepsilon_4) e^{\vartheta_4} \\ J_5 &= D'_1 E'_2 F'_1 G'_1 e^{\vartheta_5} = D_1 G_1 (\varepsilon_3^2 + (\varepsilon_4 - \varepsilon_2) \varepsilon_3 - \varepsilon_2 \varepsilon_4) e^{\vartheta_5} \\ J_6 &= D'_1 E'_2 F'_2 G'_2 e^{\vartheta_6} = D_1 G_2 (-\varepsilon_3^2 + (\varepsilon_4 + \varepsilon_2) \varepsilon_3 - \varepsilon_2 \varepsilon_4) e^{\vartheta_6} \\ J_7 &= D'_1 E'_1 F'_2 G'_1 e^{\vartheta_7} = D_1 G_1 (-\varepsilon_3^2 + (\varepsilon_4 - \varepsilon_2) \varepsilon_3 + \varepsilon_2 \varepsilon_4) e^{\vartheta_7} \\ J_8 &= D'_1 E'_1 F'_1 G'_2 e^{\vartheta_8} = D_1 G_2 (\varepsilon_3^2 + (\varepsilon_4 + \varepsilon_2) \varepsilon_3 + \varepsilon_2 \varepsilon_4) e^{\vartheta_8} \\ D_1 &= \varepsilon_2 + 1 \\ D_2 &= \varepsilon_2 - 1 \\ G_1 &= 1 + \varepsilon_4 \\ G_2 &= 1 - \varepsilon_4 \\ \vartheta_1 &= \vartheta_8 = -2k_x (2d_1) \\ \vartheta_2 &= \vartheta_5 = -2k_x (3d_1) \\ \vartheta_4 &= \vartheta_7 = -2k_x (d_1) \\ \vartheta_3 &= 0 \end{aligned}$$

So the transmission coefficient and reflection coefficient can be

represented

$$T = \frac{16\varepsilon_2\varepsilon_4 e^{k_x d_{l3}}}{[A(\varepsilon'^2 - \varepsilon''^2) + B\varepsilon' + C]^2 + [2A\varepsilon'\varepsilon'' + B\varepsilon'']^2} [(A\varepsilon'^3 + B\varepsilon'^2 + C\varepsilon' + (B + A\varepsilon')\varepsilon''^2) + i(C - A(\varepsilon'^2 + \varepsilon''^2))] = T' + iT'' \tag{2}$$

$$R = \frac{A'(\varepsilon' + i \times \varepsilon'')^2 + B'(\varepsilon' + i \times \varepsilon'') + C'}{A(\varepsilon' + i \times \varepsilon'')^2 + B(\varepsilon' + i \times \varepsilon'') + C} \tag{3}$$

where

$$\begin{aligned} A &= -\left((\varepsilon_2 + 1)(1 + \varepsilon_4) + (\varepsilon_2 - 1)(1 - \varepsilon_4) e^{-2k_x(4d_1)}\right) \\ &\quad + 2(\varepsilon_2 + \varepsilon_4) e^{-2k_x(2d_1)} - 2(1 - \varepsilon_2\varepsilon_4) e^{-2k_x(3d_1)} \\ &\quad + 2(1 - \varepsilon_2\varepsilon_4) e^{-2k_x(d_1)} \\ B &= \left((\varepsilon_2 + 1)(1 + \varepsilon_4) + (\varepsilon_2 - 1)(1 - \varepsilon_4) e^{-2k_x(4d_1)}\right) (\varepsilon_2 + \varepsilon_4) \\ &\quad + 2(\varepsilon_2 + \varepsilon_4)^2 e^{-2k_x(2d_1)} - 2(\varepsilon_4 - \varepsilon_2)^2 e^{-2k_x(3d_1)} \\ &\quad - 2(\varepsilon_4 - \varepsilon_2)^2 e^{-2k_x(d_1)} \\ C &= \left(-\left((\varepsilon_2 + 1)(1 + \varepsilon_4) + (\varepsilon_2 - 1)(1 - \varepsilon_4) e^{-2k_x(4d_1)}\right) \right. \\ &\quad \left. + 2(\varepsilon_2 + \varepsilon_4) e^{-2k_x(2d_1)} + 2(1 - \varepsilon_2\varepsilon_4) e^{-2k_x(3d_1)} \right. \\ &\quad \left. - 2(1 - \varepsilon_2\varepsilon_4) e^{-2k_x(d_1)}\right) \varepsilon_2\varepsilon_4 \\ A' &= -\left((\varepsilon_2 - 1)(1 + \varepsilon_4) + (\varepsilon_2 + 1)(1 - \varepsilon_4) e^{-2k_x(4d_1)}\right) \\ &\quad + 2(\varepsilon_2 - \varepsilon_4) e^{-2k_x(2d_1)} + 2(1 + \varepsilon_2\varepsilon_4) e^{-2k_x(3d_1)} \\ &\quad - 2(1 + \varepsilon_2\varepsilon_4) e^{-2k_x(d_1)} \\ B' &= \left((\varepsilon_2 - 1)(1 + \varepsilon_4) + (\varepsilon_2 + 1)(1 - \varepsilon_4) e^{-2k_x(4d_1)}\right) (\varepsilon_2 + \varepsilon_4) \\ &\quad + 2(\varepsilon_2^2 - \varepsilon_4^2) e^{-2k_x(2d_1)} + 2(\varepsilon_4^2 - \varepsilon_2^2) e^{-2k_x(3d_1)} \\ &\quad + 2(\varepsilon_4^2 - \varepsilon_2^2) e^{-2k_x(d_1)} \\ C' &= \left(-\left((\varepsilon_2 - 1)(1 + \varepsilon_4) + (\varepsilon_2 + 1)(1 - \varepsilon_4) e^{-2k_x(4d_1)}\right) \right. \\ &\quad \left. + 2(\varepsilon_2 - \varepsilon_4) e^{-2k_x(2d_1)} - 2(1 + \varepsilon_2\varepsilon_4) e^{-2k_x(3d_1)} \right. \\ &\quad \left. + 2(1 + \varepsilon_2\varepsilon_4) e^{-2k_x(d_1)}\right) \varepsilon_2\varepsilon_4 \end{aligned}$$

So the phase transfer function (PTF) can be expressed:

$$\begin{aligned} \text{PTF} &= \tan^{-1}(T''/T') \\ &= \tan^{-1}((C - A(\varepsilon'^2 + \varepsilon''^2))/(A\varepsilon'^3 + B\varepsilon'^2 + C\varepsilon' + (B + A\varepsilon')\varepsilon''^2)) \end{aligned} \quad (4)$$

The argument of \tan^{-1} term is supposed to be zero for zero-PTF condition, which means the phase difference is zero in the image plane. Now, the zero-PTF matching condition is discussed. By making Eq. (4) to be zero, we can obtain the constraint relations for zero-PTF:

$$\varepsilon'^2 + \varepsilon''^2 = 1 \quad (5)$$

$$1 - \varepsilon_2\varepsilon_4 = 0 \quad (6)$$

Next, we can get the constraint conditions for minimum reflectivity by using the reflection coefficient formula. By making Eq. (3) to be the minimum value, the constraint condition for minimum reflectivity can be obtained

$$\varepsilon' = -(A'C - AC') \quad (7)$$

$$\varepsilon'' = \sqrt{(A'B - AB')(B'C - BC') - (A'C - AC')^2} \quad (8)$$

The wavevector relation can be expressed as

$$(k_x)^2 + (k_z^j)^2 = \varepsilon_j\mu(\omega/c)^2 \quad (j = 2, 3) \quad (9)$$

The superlens can enhance evanescent waves to achieve super-resolution by existing Surface Plasmon Wave (SPW) on the two interfaces of metal/medium. In order to analyze the superlens work, we get the dispersion relation of SPW by using the boundary conditions and Eq. (9)

$$k_z^{(3)}d_2 = \frac{1}{2} \ln \left| \frac{\left(1 - \frac{\varepsilon_4 k_z^{(3)}}{\varepsilon_3 k_z^{(4)}}\right) \left(\frac{\varepsilon_3 k_z^{(2)}}{\varepsilon_2 k_z^{(3)}} - 1\right)}{\left(1 + \frac{\varepsilon_4 k_z^{(3)}}{\varepsilon_3 k_z^{(4)}}\right) \left(1 + \frac{\varepsilon_3 k_z^{(2)}}{\varepsilon_2 k_z^{(3)}}\right)} \right| \quad (10)$$

when $d \rightarrow \infty$, $\frac{\varepsilon_3 k_z^{(2)}}{\varepsilon_2 k_z^{(3)}} = 1$ or $\frac{\varepsilon_4 k_z^{(3)}}{\varepsilon_3 k_z^{(4)}} = 1$, and we can obtain

$$\frac{c^2 \left(k_x^{(+)}\right)^2}{\omega^2} = \left| \frac{\varepsilon_2 \varepsilon_3}{\varepsilon_2 + \varepsilon_3} \right|, \quad \frac{c^2 \left(k_x^{(-)}\right)^2}{\omega^2} = \left| \frac{\varepsilon_4 \varepsilon_3}{\varepsilon_4 + \varepsilon_3} \right| \quad (11)$$

where $k_x^{(+)}$ and $k_x^{(-)}$ are the transverse wave vector on the top or bottom Ag slab, separately.

So, when $d_2 \rightarrow \infty$, both two interfaces can exist SPW, and these SPW are uncorrelated each other; when d_2 is small, these SPW are coupled and split into two modes, i.e., the symmetric mode and antisymmetric mode, in the thin metal film [27–32].

3. NUMERICAL SIMULATIONS

The software of COMSOL Multiphysics and Matlab are used for simulation. In following figures, the units of x and z are meter. Here we use the following parameters: The thickness of Ag slab is 30 nm [22, 33], and the thicknesses of ARPC coating are 15 nm. Firstly, we discuss the constraint relations for zero-PTF. Figure 2 shows the PTF of the ARPC-superlens as a function of k_x/k_0 when the Eq. (5) is satisfied or isn't satisfied, respectively. And $\varepsilon'^2 + \varepsilon''^2 = 1$ can be realized by changing the working wavelength [22, 23]. It is obvious that the PTF approaches zero after the off-resonance regime while the spatial frequency (k_x/k_0) increases when $\varepsilon_2\varepsilon_4$ and $\varepsilon'^2 + \varepsilon''^2$ tend to be one. These conclusions reconfirm that the phase can be retrieved in the control of the constraint relations for zero-PTF, and the results are consistent with Ref. [22].

Following, we further discuss the constraint conditions for minimum reflectivity. Figure 3 shows the values of ε_3 depending on ε_2 ($\varepsilon_4 = 1/\varepsilon_2$), which are calculated by Eqs. (7) and (8). It is obvious that $|\varepsilon'| > 1$, so Eq. (5) is not satisfied. When the minimum phase difference need to be satisfied, the range of ε_2 is 1.1 \sim 1.5 in order to satisfy constraint relations for zero-PTF. And Figure 4 shows $|R|$ as a function of k_x/k_0 depending on the different permittivity of ARPC-superlens. ARPC can effectively reduce the reflectivity while the spatial frequency (k_x/k_0) increases. The reason is that the surface plasmon resonance (SPR) is increased. Because of significant intrinsic loss ($\varepsilon'' > 0$), the impedance-mismatched cases can exist SPR to improve the near-field

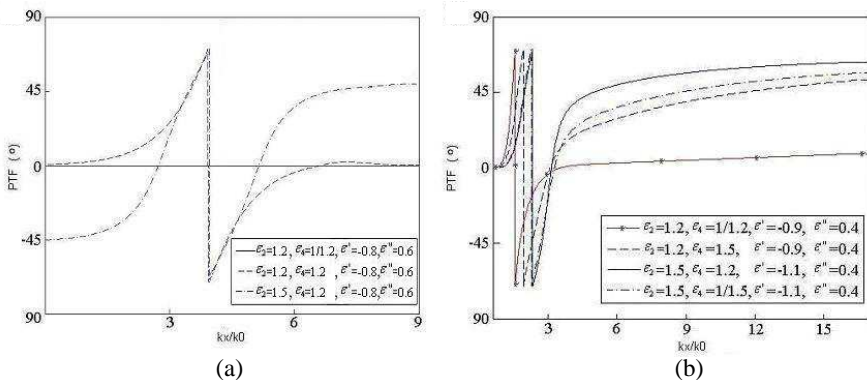


Figure 2. The PTF of the ARPC-superlens model is depicted vs. k_x/k_0 corresponding to virtually changing ε_2 , ε_4 , ε_3 .

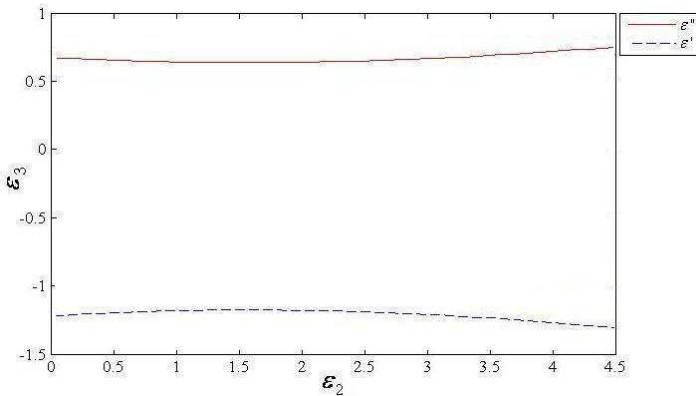


Figure 3. The relationship for permittivity of ARPC and the superlens.

image [23, 34, 35]. The ARPC coatings will change the optical path of superlens. The mismatched dielectric allows the SPR towards larger values of the evanescent wavevector, which are associated with surface plasmons that propagate parallel to the metal/ARPC interfaces. The ARPC coatings reduce the oscillations in the reflectance and make more energy to exist SPR. So, more evanescent waves will participate in the imaging process. This is beneficial for the formation of high resolution images with superlensing process, as shown in Figure 5. From the Figure 4 and Figure 5, we can obtain that there are higher transmittance of evanescent wave under the constraint relations for zero-PTF compared to the superlens without ARPC. The higher transmittance and zero-PTF can be realized at the same time, which can improve super-resolution.

Following, Figures 6(a) and (b) show the magnetic field intensity distribution of the ARPC superlens and a superlens without ARPC, respectively. It is obvious that the magnetic field intensity of ARPC superlens is stronger. And this reconfirms the above conclusions.

Lastly we examine the imaging resolution on an image plane. Figure 7 shows the lateral intensity distributions through the double slits of 20 nm slit width. Whether the double-slit can be distinguished in the image plane is dependent on the minimum value of intensity at the central location. So the employment of ARPC can effectively improve the image visibility. And by using the image contrast formula

$$C = \frac{I_{\max} - I_{\min}}{I_{\max} + I_{\min}} \quad (12)$$

we can obtain that the image contrast of ARPC-superlens is about 0.61,

compared to 0.38 of the superlens without ARPC, so the image contrast can be greatly improved by ARPC. The reason is that intrinsic loss of absorption in the Ag slab superlens turn out to add a blurring effect

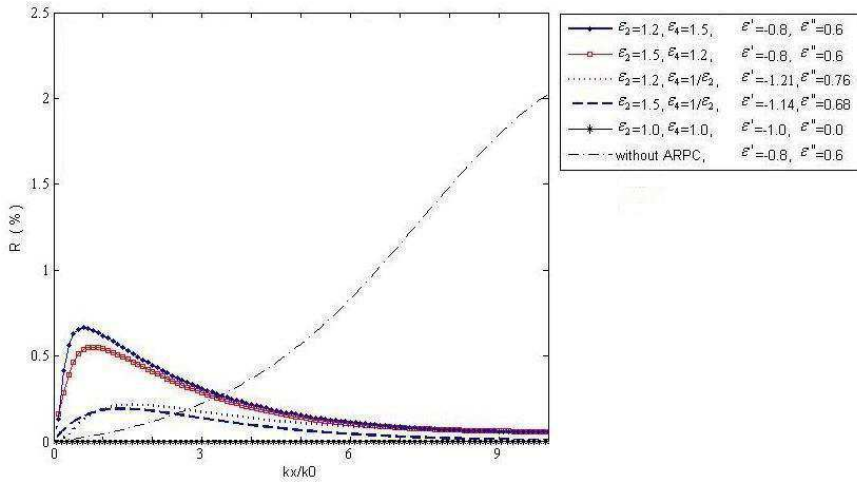


Figure 4. The reflectivity of the ARPC superlens imaging model is depicted vs k_x/k_0 corresponding to virtually changing ϵ_2 , ϵ_4 , ϵ_3 .

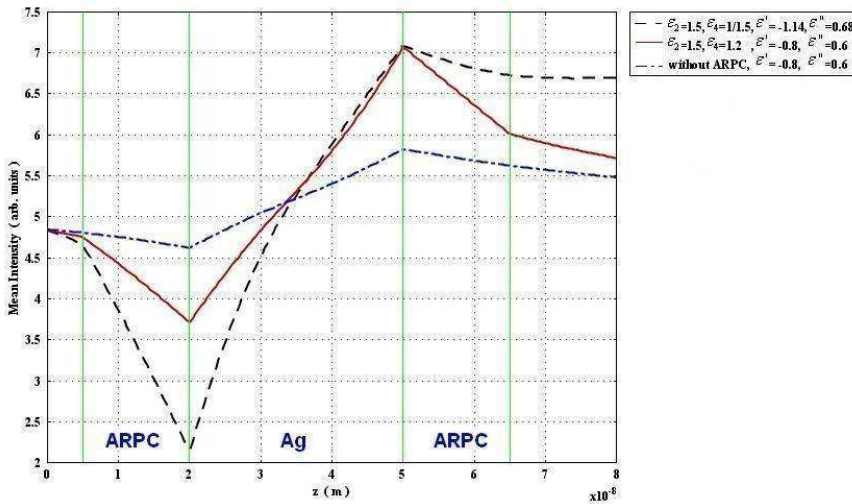


Figure 5. The integrated mean intensity of the ARPC superlens image.

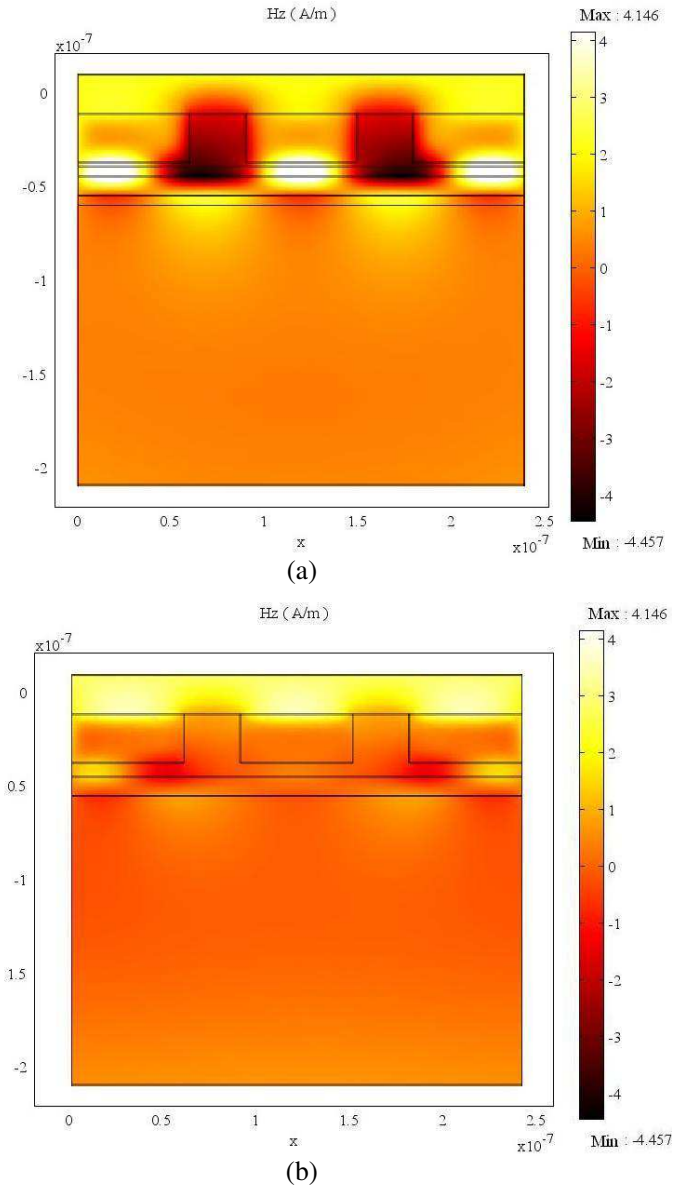


Figure 6. (a) The magnetic field intensity distribution of the ARPC superlens. (b) The magnetic field intensity distribution of a superlens without ARPC.

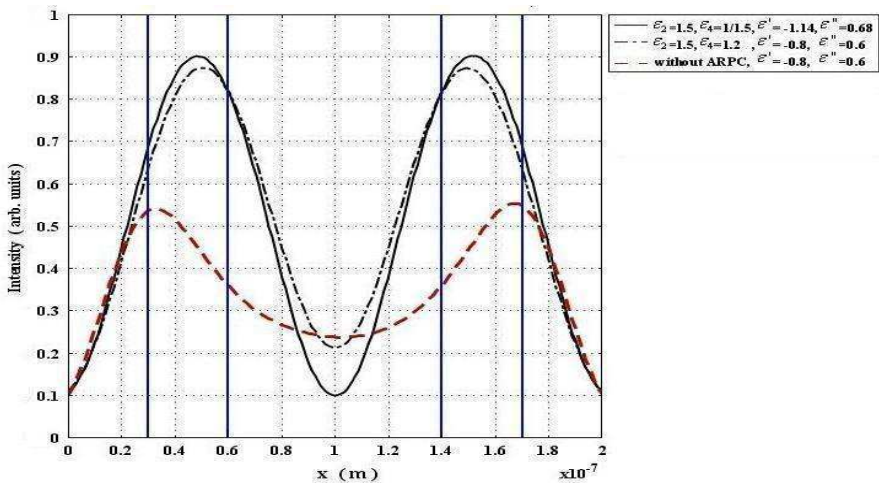


Figure 7. The lateral intensity distributions through a 20 nm width double slit.

to the ideal image reconstruction for the impedance match case [23], so the optimized image quality can be obtained with the impedance mismatch case. Therefore the ARPC can reduce the reflectivity and make the PTF to approach zero at the same time.

4. CONCLUSION

In conclusion, we successfully applied ARPC to superlens imaging system and verified the significant enhancement of the image contrast and resolving capability. ARPC is capable of reducing the reflectivity of superlens surface and making phase difference approaching zero at the same time. This model is believed to be applicable to optical nanoimaging, nanolithography, and biomedical sensing.

ACKNOWLEDGMENT

Supported by the Fundamental Research Funds for the Central Universities (lzujbky-2009-165).

REFERENCES

1. Pendry, J. B., "Negative refraction makes a perfect lens," *Phys. Rev. Lett.*, Vol. 85, 3966, 2000.

2. Pokrovsky, A. L. and A. L. Efros, "Lens based on the use of left-handed materials," *Appl. Opt.*, Vol. 42, 5701–5705, 2003.
3. Gong, Y. and G. Wang, "Superficial tumor hyperthermia with flat left-handed metamaterial lens," *Progress In Electromagnetics Research*, Vol. 98, 389–405, 2009.
4. Wang, G., Y. Gong, and H. Wang, "On the size of left-handed material lens for near-field target detection by focus scanning," *Progress In Electromagnetics Research*, Vol. 87, 345–361, 2008.
5. Xi, S., H. Chen, B.-I. Wu, and J. A. Kong, "Experimental confirmation of guidance properties using planar anisotropic left-handed metamaterial slabs based on s-ring resonators," *Progress In Electromagnetics Research*, Vol. 84, 279–287, 2008.
6. Gong, Y. and G. Wang, "Superficial tumor hyperthermia with flat left-handed metamaterial lens," *Progress In Electromagnetics Research*, Vol. 98, 389–405, 2009.
7. Veselago, V. G., "Properties of materials having simultaneously negative values of dielectric (ϵ) and magnetic (μ) susceptibilities," *Sov. Phys. Solid State*, Vol. 8, 2854–2856, 1967.
8. Zhang, Y., T. M. Grzegorzczuk, and J. A. Kong, "Propagation of electromagnetic waves in a slab with negative permittivity and negative permeability," *Progress In Electromagnetics Research*, Vol. 35, 271–286, 2002.
9. Qiao, S., G. A. Zheng, and L. X. Ran, "Enhancement of evanescent wave in an electrically anisotropic slab with partially negative permittivity tensor," *Journal of Electromagnetic Waves and Applications*, Vol. 22, No. 10, 1341–1350, 2008.
10. Mahmoud, S. F. and A. J. Viitanen, "Surface wave character on a slab of metamaterial with negative permittivity and permeability," *Progress In Electromagnetics Research*, Vol. 51, 127–137, 2005.
11. Mikki, S. M. and A. A. Kishk, "Electromagnetic wave propagation in nonlocal media: Negative group velocity and beyond," *Progress In Electromagnetics Research B*, Vol. 14, 149–174, 2009.
12. Zhu, X., W.-Y. Pan, and B.-R. Guan, "Electromagnetic field generated by a horizontal electric dipole on a double negative medium half space," *Progress In Electromagnetics Research M*, Vol. 6, 123–137, 2009.
13. Lee, H., Y. Xiong, N. Fang, W. Srituravanich, S. Durant, M. Ambati, C. Sun, and X. Zhang, "Realization of optical superlens imaging below the diffraction limit," *New Journal of Physics*, Vol. 7, 2005.
14. Liu, Z. W., N. Fang, T.-J. Yen, and X. Zhang, "Rapid growth of

- evanescent wave by a silver superlens,” *Appl. Phys. Lett.*, Vol. 83, 5184, 2003.
15. Rao, X. S. and C. K. Ong, “Subwavelength imaging by a left-handed material superlens,” *Phys. Rev. E*, Vol. 68, 067601, 2003.
 16. Moore, C. P., M. D. Arnold, P. J. Bones, and R. J. Blaikie, “Image fidelity for single-layer and multi-layer silver superlenses,” *JOSA A*, Vol. 25, No. 4, 911–918, 2008.
 17. Shi, Z., V. Kochergin, and F. Wang, “193 nm superlens imaging structure for 20 nm lithography node,” *Optics Express*, Vol. 17, No. 14, 11309–11314, 2009.
 18. Chaturvedi, P., W. Wu, V. J. Logeeswaran, Z. N. Yu, M. S. Islam, S. Y. Wang, R. S. Williams, and N. X. Fang, “A smooth optical superlens,” *Appl. Phys. Lett.*, Vol. 96, 043102, 2010.
 19. Taubner, T., D. Korobkin, Y. Urzhumov, G. Shvets, and R. Hillenbrand, “Near-field microscopy through a SiC superlens,” *Science*, Vol. 313, 1595, 2006.
 20. Fang, N., H. Lee, C. Sun, and X. Zhang, “Sub-diffraction-limited optical imaging with a silver superlens,” *Science*, Vol. 308, 534, 2005.
 21. Cai, W., D. A. Genov, and V. M. Shalaev, “Superlens based on metal-dielectric composites,” *Phys. Rev. B*, Vol. 72, 193101, 2005.
 22. Lee, K., Y. Jung, G. Kang, H. Park, and K. Kim, “Active phase control of a Ag near-field superlens via the index mismatch approach,” *Appl. Phys. Lett.*, Vol. 94, 101113, 2009.
 23. Lee, K., H. Park, J. Kim, G. Kang, and K. Kim, “Improved image quality of a Ag slab near-field superlens with intrinsic loss of absorption,” *Optics Express*, Vol. 16, No. 3, 1711–1718, 2008.
 24. Ramakrishna, S. A., J. B. Pendry, M. C. K. Wiltshire, and W. J. Stewart, “Imaging the near field,” *J. Mod. Opt.*, Vol. 50, 1419–1430, 2003.
 25. Cao, P. F., X. P. Zhang, L. Cheng, and Q. Q. Meng, “Far field imaging research based on multilayer positive- and negative-refractive-index media under off-axis illumination,” *Progress In Electromagnetics Research*, Vol. 98, 283–298, 2009.
 26. Ye, Z., “Optical transmission and reflection of perfect lenses by left handed materials,” *Physical Review B*, Vol. 67, 193106, 2003.
 27. Dong, J., “Surface wave modes in chiral negative refraction grounded slab waveguides,” *Progress In Electromagnetics Research*, Vol. 95, 153–166, 2009.
 28. Kong, F., K. Li, H. Huang, B.-I. Wu, and J. A. Kong, “Analysis of the surface magnetoplasmon modes in the semiconductor slit

- waveguide at terahertz frequencies,” *Progress In Electromagnetics Research*, Vol. 82, 257–270, 2008.
29. Shi, Y. and C. H. Chan, “Solution to electromagnetic scattering by Bi-isotropic media using multilevel Green’s function interpolation method,” *Progress In Electromagnetics Research*, Vol. 97, 259–274, 2009.
 30. Zia, R., M. D. Selker, P. B. Catrysse, and M. L. Brongersma, “Geometries and materials for subwavelength surface plasmon modes,” *J. Opt. Soc. Am. A*, Vol. 21, No. 12, 2442–2446, 2004.
 31. Yun, B. F., G. H. Hu, and Y. P. Cui, “Bound modes analysis of symmetric dielectric loaded surface plasmon-polariton waveguides,” *Optics Express*, Vol. 17, No. 5, 3610–3618, 2009.
 32. Berini, P., “Figures of merit for surface plasmon waveguides,” *Optics Express*, Vol. 14, No. 26, 13030–13042, 2006.
 33. Liu, Z. W., N. Fang, T. J. Yen, and X. Zhang, “Rapid growth of evanescent wave by a silver superlens,” *Appl. Phys. Lett.*, Vol. 83, 5184, 2003.
 34. Yang, X. F., Y. Liu, J. X. Ma, J. H. Cui, H. Xing, W. Wang, C. T. Wang, and X. G. Luo, “Broadband super-resolution imaging by a superlens with unmatched dielectric medium,” *Optics Express*, Vol. 16, No. 24, 19686–19694, 2008.
 35. Karalis, A., E. Lidorikis, M. Ibanescu, J. D. Joannopoulos, and M. Soljagic, “Surface-plasmon-assisted guiding of broadband slow and subwavelength light in air,” *Phys. Rev. Lett.*, Vol. 95, 063901, 2005.